

Rafał LEWKOWICZ ORCID 0000-0003-3691-6558, rlewkowicz@wiml.waw.pl  
*Military Institute of Aviation Medicine (Wojskowy Instytut Medycyny Lotniczej), Poland*

## AN AVIATION ACCIDENT REPORT DATA-DRIVEN APPROACH TO SCENARIO DESIGN FOR A CENTRIFUGE-BASED DYNAMIC FLIGHT SIMULATOR

**Podejście oparte na danych z raportu o wypadku lotniczym  
do projektowania scenariuszy dla dynamicznego symulatora  
lotu bazującego na wirówce przeciążeniowej**

**Abstract:** The use of flight simulators in investigating an aviation incident or accident related to human errors has been identified as an important part of a strategy to improve safety. This study aimed to replicate a real flight of the MiG-29 aircraft using a centrifuge-based dynamic flight simulator and to determine the simulator's accuracy in recreating in-flight aircraft performance. A 60-second recording of the real flight of the MiG-29 aircraft, captured by the flight data recorder, was chosen for replication in the HTC-07 human training centrifuge simulator. To evaluate how accurately the simulator replicates the performance of the aircraft, the linear accelerations and angular velocities acting on a pilot during the real flight were compared with those during the replication of that flight in the simulator. The fit of these parameters was assessed using the root mean square percentage error (RMSPE) and the correlation coefficient ( $r$ ). The highest replication accuracy was achieved for the vertical component of the linear acceleration (RMSPE=2068;  $r=0.98$ ), while the worst result was obtained for the longitudinal component (RMSPE=14205;  $r=0.31$ ). Inaccuracies were much more pronounced for the angular velocity. The roll angular velocity had the lowest replication error (RMSPE=12640). However, its correlation with the recorded velocity during the real flight was very weak ( $r=-0.02$ ). Despite some inaccuracies in replicating other components of the acceleration and angular velocity vectors, the HTC-07 simulator seems valuable for investigating aviation incidents or accidents related to human factors.

**Keywords:** human factor, flight simulator, centrifuge, flight safety, accident investigation



**Streszczenie:** Wykorzystanie symulatorów lotu w badaniach incydentu lub wypadku lotniczego, którego przyczyną mógł być błąd ludzki, zostało uznane za ważną część strategii poprawy bezpieczeństwa lotów. Celem tego badania było odtworzenie rzeczywistego lotu samolotu MiG-29 w dynamicznym symulatorze lotu opartym na wirówce przeciążeniowej oraz ocena, czy symulator ten może dokładnie odtworzyć osiągi samolotu podczas lotu. Do odtworzenia w wirówce przeciążeniowej – symulatorze HTC-07 wybrano 60-sekundowe nagranie rzeczywistego lotu samolotu MiG-29, zarejestrowane przez pokładowy rejestrator danych lotu. W celu oceny, jak dokładnie symulator odtwarza osiągi samolotu porównano przyspieszenia liniowe i prędkości kątowe działające na pilota podczas rzeczywistego lotu z przyspieszeniami działającymi podczas replikacji tego lotu w symulatorze. Dopasowanie tych parametrów oceniono za pomocą średniokwadratowego błędu procentowego (RMSPE) oraz współczynnika korelacji ( $r$ ). Największą dokładność replikacji osiągnęła składowa pionowa przyspieszenia liniowego (RMSPE = 2068;  $r = 0,98$ ), podczas gdy najgorszy wynik miała składowa podłużna (RMSPE = 14205;  $r = 0,31$ ). Niedokładności były znacznie bardziej widoczne w przypadku prędkości kątowej. Prędkość kątowa przechiły miała najwyższy błąd replikacji (RMSPE = 12640), jednak jej korelacja z zarejestrowaną prędkością podczas rzeczywistego lotu była bardzo słaba ( $r = -0,02$ ). Pomimo niedokładności w odtwarzaniu pozostałych składowych wektorów przyspieszenia i prędkości kątowej, symulator HTC-07 wydaje się cennym narzędziem do badania incydentów lub wypadków lotniczych związanych z czynnikiem ludzkim.

**Słowa kluczowe:** czynnik ludzki, symulator lotu, wirówka, bezpieczeństwo lotu, badanie wypadku

Received: November 22, 2023/ Revised: November 30, 2023/ Accepted: December 13, 2023/ Published: December 28, 2023

### Nomenclature:

$O_hx_hy_hz_h$	– frame of reference fixed to the pilot's head
$O_ex_ey_ez_e$	– earth-centered earth-fixed (ECEF) coordinate system
$O_nx_ny_nz_n$	– local North-East-Down (NED) coordinate system
$O_anx_any_anz_an$	– aircraft-carried NED system
$O_bx_by_bz_b$	– body frame of reference fixed to the aircraft
$Ax_Ay_Az_A$	– frame of reference fixed to the arm of the motion platform
$Rx_Ry_Rz_R$	– frame of reference fixed to the ring of the motion platform
$Cx_Cy_Cz_C$	– frame of reference fixed to the simulator cabin
$\phi, \theta, \psi$	– Euler angles (roll, pitch and yaw, respectively)
$a_{xi}, a_{yi}, a_{zi}$	– linear acceleration vector in $i$ -th reference system, along x-, y-, and z-axis, respectively
$p_i, q_i, r_i$	– roll, pitch and yaw rate of $i$ -th frame of reference, respectively
$\Omega_i$	– angular velocity vector of $i$ -th frame of reference
$\mathbf{b}$	– vector of actual flight parameters replicated in the simulator

<b>k</b>	– vector of the simulator cabin kinematics
<b>l<sub>h</sub></b>	– distance vector between the origins of the head-fixed and the aircraft body frames
<b>g</b>	– acceleration of the earth's gravity
<i>Superscript</i>	
<b>htc</b>	– represents variable related to the HTC-07 simulator
<b>ac</b>	– represents variable related to the aircraft
<i>Subscript</i>	
<b>n</b>	– represents coordinate vectors in the local NED coordinate system
<b>an</b>	– represents coordinate vectors in the aircraft-carried NED coordinate system
<b>b</b>	– represents coordinate vectors expressed in the body frame
<b>C</b>	– represents coordinate vectors expressed in the simulator cabin frame
<b>h</b>	– represents coordinate vectors expressed in the head-fixed frame
<b>e</b>	– represents coordinate vectors expressed in the ECEF coordinate system

## 1. Introduction

Recreating the conditions and sequence of a pilot's actions during a critical phase of flight is usually risky and costly when done during a real flight. As a result, various forms of simulation play a key role in accident investigations [1], [2]. The replication of conditions from the critical phase of flight in a flight simulator is mainly based on data from the flight data recorder (FDR) [3]. While most flight simulators have a feature that allows data from a simulated flight to be recorded and then played back, few are designed to play back data recorded during a real flight [4]. In addition, due to certain limitations, such as poor motion cueing, simulators do not always provide a high-fidelity recreation of real flight conditions. It should also be noted that the reliability of such simulations depends mainly on whether they are based on flight data that has been properly measured and recorded during a real flight.

Data from various sources, including an FDR, a cockpit voice recorder, and eyewitness information, are collected [5], [6] to reconstruct the real flight. Although these data are often crucial to explain the sequence of events leading up to the accident, they do not always provide an explanation of a pilot's behavior. Only a thorough analysis of the flight and the conditions in which it took place will allow us to assess the pilot's behavior and identify the cause of the pilot's error. Therefore, one of the strategies used to tackle accident rates is a data-driven approach that enhances the quantity and quality of information gathered during accident investigations [7]–[9].

The use of simulators is an important part of a strategy aimed at improving flight safety, particularly in the use of modelling and simulation to support training that reduces accidents, and research to support the analysis of aviation mishaps [3]. However, not every simulator can assist in investigating an accident where a pilot has flown with high and sustained accelerations (G-forces). Indeed, G-forces, affecting the pilot mainly in fast-jet aircraft, are an important flight safety issue. In-flight accelerations can cause visual disturbances (e.g., tunnel vision or blackout) in a pilot, which result from a shifting of blood from the head to the lower limbs and are a symptom of approaching loss of consciousness. The studies [10] and [11] indicated that acceleration not only adversely affected retinal oxygenation but also impaired the functioning of the central nervous system. The effects of these disturbances include increased reaction time to a light stimulus [12], [13], increased color perception threshold [14]–[16], altered perception of the critical fusion frequency of the light stimulus [17], [18], cognitive functions [19], and night vision [20]. In extreme cases, the pilot may experience G-force-induced loss of consciousness (G-LOC) or almost loss of consciousness (A-LOC), a condition insufficient to cause G-LOC but involves a significant reduction in a pilot's cognitive and/or physiological functions [21]. They may occur due to reduced pilot tolerance to acceleration (influenced by a wide variety of factors [22]–[24]) or poor Anti-G Straining Maneuver (AGSM) performance.

A specialized centrifuge-based flight simulator can be used to investigate the accident of a fast jet aircraft and to determine the cause of a possible pilot error. This so-called human training centrifuge (HTC) is a dynamic flight simulator that provides high, rapid onset, and sustained accelerations similar to those experienced by pilots in real flight [25]. In recent studies, the use of the HTC to recreate real in-flight conditions was shown to be a unique way to support an incident investigation [26] or pilot training [25]. The study [26] found that the HTC is capable of replicating quite accurately the +Gz acceleration experienced by a pilot during a real flight in the F-16 aircraft. Based on the results of previous research [26] and the fact that the HTC is also equipped with a replica of the cockpit of a MiG-29 aircraft, this paper presents the method of replicating the actual flight of this type of aircraft.

## **1.1. The aim of the study**

The presented study aimed to replicate the real flight of the MiG-29 aircraft in the human training centrifuge (HTC) – a dynamic flight simulator - and assess quantitatively and qualitatively whether the simulator can accurately recreate in-flight aircraft performance.

This study addressed the problem associated with the real flight replication in the HTC, using data from a flight data recorder (FDR). The proposed approach can provide new insights into the flight data and determine whether the in-flight acceleration (G-forces) may have contributed to, e.g., a pilot's visual disturbance. Therefore, the results of this study

may be useful in the applying the HTC to aircraft accident investigations, especially by those who use simulators with a similar design and control system.

## 2. Methods

### 2.1. Flight simulator

The human training centrifuge HTC-07 (AMST-Systemtechnik GmbH, Austria) (Fig. 1) located at the Military Institute of Aviation Medicine (WIML, Poland) was used to recreate a real flight of the MiG-29 aircraft. This dynamic flight simulator combines the functions of a flight simulator and a centrifuge, which is used both for pilot training and assessing how pilots tolerate high and sustained accelerations (G-forces).

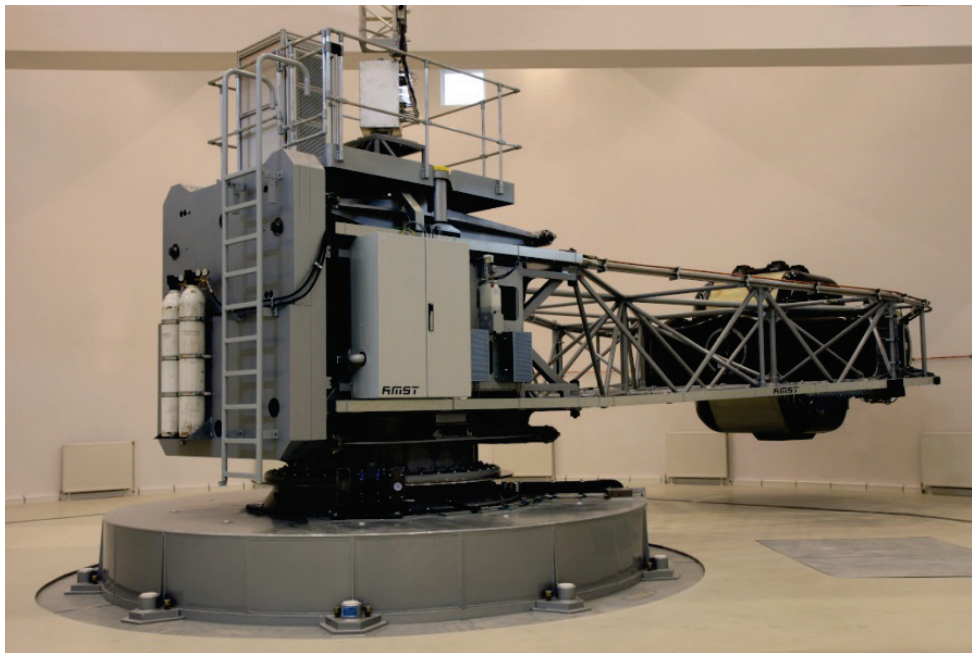


**Fig. 1.** Dynamic flight simulator – HTC-07

The simulator cockpit can replicate the cockpit of F-16 Block 52+ and MiG-29 aircraft. This option allows the pilot to perform tasks currently available in a traditional flight simulator, including pre-flight procedures, instrument and navigation flight as well as approaches to landing according to VOR, VOR/DME, NDB, ILS and TACAN, operation of communications equipment, night flight procedures, group flying and navigation in

adverse weather conditions. In addition, the simulator provides upset prevention and recovery training, emergency training (engine fire, control system failure) and combat applications training (interception of airborne targets, defensive maneuvers, use of weapons) [27].

The motion system of the HTC-07 simulator has 3 degrees of freedom with the cabin mounted on an 8-metre arm. The motion system design allows linear accelerations to be generated simultaneously in three axes. The range of acceleration generated and the limitations of the simulator kinematics are shown in Table 1.

**Table 1**  
**Kinematics parameters of the HTC-07 simulator motion system [28]**

Parameter	$O_c x_c^*$	$O_c y_c^*$	$O_c z_c^*$
Range of motion in relation to axis [deg]	-	$\pm 360$	$\pm 360$
Maximum linear acceleration [G]	16 / -3	$\pm 6$	$\pm 10$
Maximum linear acceleration onset rate [G/s]	14.5	6	10
Maximum angular acceleration onset rate [rad/s <sup>2</sup> ]	2.82	8	5

\* – axis of the coordinate frame associated with the simulator cabin (frame defined in the next section of the paper)

G – the resultant inertial forces; its magnitude is equal to the earth's gravitational acceleration ( $g = 1G \sim 9.81 \text{ m/s}^2$ )

The HTC-07 simulator allows the replication of any MiG-29 and F-16 aircraft flight scenarios, but the simulator's manufacturer has not provided data to confirm the accuracy of this replication. The HTC-07 simulator user manual [28] defines 10 parameters (Tab. 2), the minimum data set required to recreate flight in the simulator. These data are separated by semicolons and stored in American Standard Code for Information Interchange (ASCII) format.

For the purposes of this research, to recreate a real flight in the HTC-07 simulator, the set of parameters shown in Table 2 has been chosen. These parameters define a vector that generates physical linear acceleration and the flight scenery imagery. To illustrate changes in the flight instruments, e.g. indicated airspeed, it is possible to include additional data beyond those listed in Table 2.

**Table 2**

**The minimum data set required to replicate a flight in the HTC-07 simulator**

Parameter	Unit	Range	Data format	Name in the source file
Time (time step 5 ms)	ms	-	double	Header.Timestamp
Linear acceleration components	$a_{x_C}^{htc}$	±6	float	MSIout.Motion.f_x_b*
	$a_{y_C}^{htc}$	±10	float	MSIout.Motion.f_y_b*
	$a_{z_C}^{htc}$	-6; +16	float	MSIout.Motion.f_z_b*
Altitude	m	-	float	MSIout.OTW.h_eye
Latitude	deg,	-90;90	double	MSIout.OTW.Lat_eye
Longitude	min, sec	-180;180	double	MSIout.OTW.Lon_eye
Time of day	h	0:24	float	MSIout.OTW.ToD
Roll angle		±π	float	MSIout.OTW.phi
Pitch angle	rad	±π/2	float	MSIout.OTW.theta
Yaw angle		±π	float	MSIout.OTW.psi

\* in the  $Cx_Cy_Cz_C$  reference frame related to the simulator cab (frame defined later in the article)

## 2.2. Study design

Replication of a real flight of the MiG-29 aircraft in the HTC-07 simulator was performed in three stages (Fig. 2). Stage 1 involved the preparation and adjustment of data from the S2-3a flight data recorder (FDR) of the MiG-29 aircraft. The next step was to replicate the developed flight scenario of the MiG-29 aircraft in the HTC-07 simulator and to record the kinematics of the simulator's motion system. In the final third stage of the study, the linear acceleration components experienced by the pilot during the real flight were compared with the corresponding accelerations recorded during the replication of that flight in the HTC-07 simulator.

Preparation of the actual flight data for the replication in the HTC-07 simulator (stage 1) was carried out according to the following procedure (Fig. 2):

- selection of parameters recorded during the real flight of the MiG-29 aircraft,
- calculation of the linear acceleration and angular velocity that acted on the pilot's head in the real flight,
- substitution of selected parameters from the real flight and calculated linear acceleration into the source file generated in the HTC-07 simulator system,
- validation of the modified data file (format, parameter values) extended to offline validation of HTC-07 simulator operation (no cab motion).

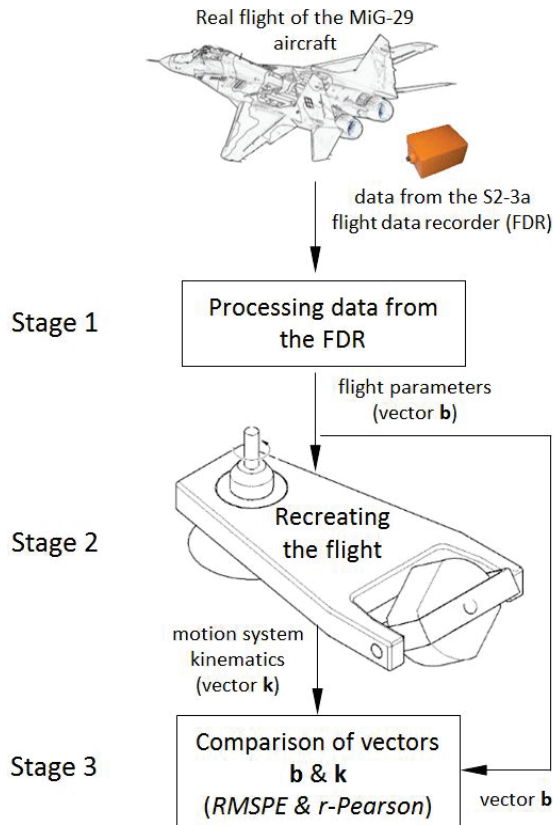


**Fig. 2.** Scheme of the replication of a real flight of a MiG-29 aircraft in the HTC-07 simulator. (FDR - flight data recorder; RMSPE – root mean square percentage error)

Replication of the MiG-29 aircraft's developed flight scenario and recording kinematics of the simulator's motion system (stage 2) was carried out using the simulator-embedded software. To compare the linear acceleration and angular velocity components experienced by the pilot in the real flight with the corresponding components recorded during the replication of this flight in the HTC-07 simulator (stage 3), two measures were used: the root mean square percentage error (RMSPE) and the r-Pearson correlation coefficient (Fig. 2).

### 2.3. A vector of parameters from an actual flight of the MiG-29 aircraft

A 60-second real flight of the MiG-29 aircraft, recorded in the memory of the S2-3a flight data recorder, was selected for replication in the HTC-07 dynamic flight simulator.

The data file chosen for an analysis contained 10 parameters, recorded at a frequency of 1 Hz. Nine parameters, shown in Table 3, were selected to create vector **b** of the real flight parameters replicated in the HTC-07 simulator.

**Table 3**

**Flight parameters stored in the memory of the S2-3a FDR**

Parameter	Unit	Reference system	Component of vector <b>b</b>	Name in the source file
Euler roll angle $\phi_b$	deg	$O_n x_n y_n z_n$ **	$\phi_{b/n}$	Gamma (+RWD)
Euler pitch angle $\theta_b$			$\theta_{b/n}$	Theta (+RWD)
Euler yaw angle $\psi_b$			$\psi_{b/n}$	Psi
Linear acceleration components	$a_{x_b}$ g $a_{y_b}$ $a_{z_b}$	$O_b x_b y_b z_b$ **	$a_h^{ac*}$	Nx Ny Nz
Altitude $h_{z_n}$	ft	$O_n x_n y_n z_n$ **	$x_n$	Hbar
True velocity $V_{x_T}$	knots	$O_b x_b y_b z_b$ **	-	Vrz
Angle of attack $\alpha$	deg	$O_b x_b y_b z_b$ **	-	a

\* – in the pilot's head-fixed coordinate system (system defined in the following subsection)

\*\* – coordinate system defined in the following subsection and in Fig. 5

\*\*\* – without gravitational acceleration component

g – the earth's gravitational acceleration ( $\sim 9.81 \text{ m/s}^2$ )

RWD – right wing down, an indicator of which direction is considered positive (+)

Figure 3 shows the aircraft angular orientation and acceleration vector components that were recorded during the actual flight of the MiG-29 aircraft (Tab. 3). The 60-second flight phase taken for the analysis included a right turn maneuvers with a roll of up to 90 degrees and the acceleration of up to +4 Gz (acceleration acting along the longitudinal axis of the pilot's body, with the direction to the lower limbs) and a left turn (from 11 seconds onwards) performed with a roll of up to 90 degrees and the acceleration of up to +7 Gz.

The in-flight recorded parameters (Fig. 3) were assumed to represent accelerations and angular velocities relative to the aircraft's center of gravity (the origin of the reference system associated with the aircraft, the system defined in the following subsection). Furthermore, despite the measurement and processing errors of the flight data recorder (S2-3a) [29], [30], the accuracy of the flight data was assumed to be sufficient to replicate in the HTC-07 simulator.

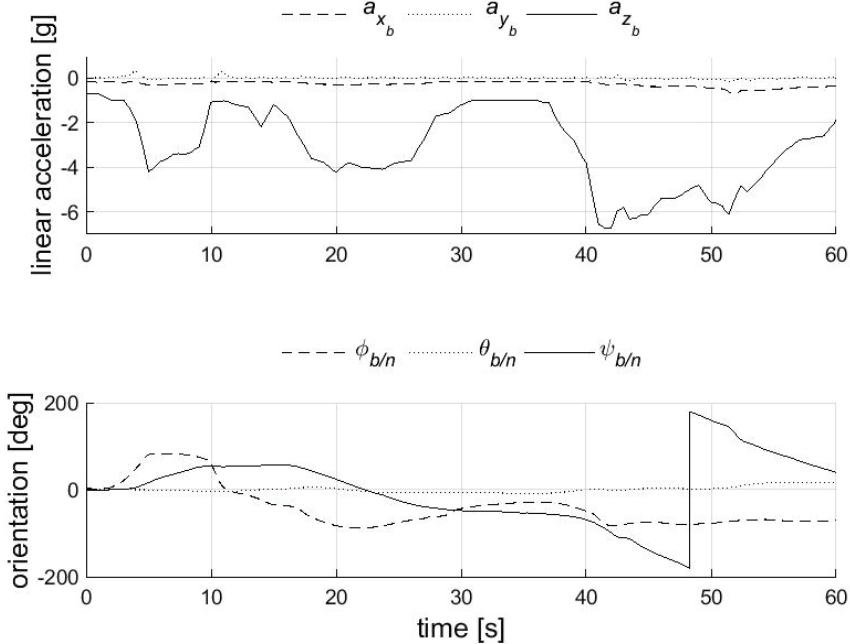


**Fig. 3.** Data from S2-3a flight data recorder (see Tab. 3 for an explanation of the data)

Taking into account the minimum data set required to replicate the real flight in the HTC-07 simulator (Tab. 2) and the parameters recorded in the real flight (Tab. 3), the vector **b** of the real flight parameters replicated in the HTC-07 simulator has the following components:

$$\mathbf{b} = [\phi_{b/n}^{ac}, \theta_{b/n}^{ac}, \psi_{b/n}^{ac}, a_{x_h}^{ac}, a_{y_h}^{ac}, a_{z_h}^{ac}, p_h^{ac}, q_h^{ac}, r_h^{ac}, \varphi, \lambda, h_{z_n}]^T \quad (1)$$

Although the components  $[p_b^{ac}, q_b^{ac}, r_b^{ac}]$  of the vector **b** (1), which represent the angular velocity of the MiG-29 aircraft, are not required to be replicated in the simulator (Tab. 2), they were included due to the need for comparison with the angular velocity components affecting the pilot in the HTC simulator cabin.

## 2.4. Linear acceleration and angular velocity acting on the MiG-29 pilot

Since the linear acceleration generated in the HTC-07 simulator is described in a frame related to the pilot's head (Tab. 2) and the acceleration recorded in the real flight is described in a frame related to the aircraft (Tab. 3), there is a need to transform the aircraft

flight data from the body coordinate system to a pilot head-fixed coordinate system. To describe the linear accelerations acting on the pilot's head in the aircraft, the following rectangular and right-handed coordinate systems are defined (Fig. 4):

- *the local North-East-Down (NED) coordinate system* (denoted by  $O_n x_n y_n z_n$ ) is a coordinate frame with the origin (denoted by  $O_n$ ) fixed to a point on the earth's surface (Fig. 5 and Fig. 4). Its axes are defined as the following (based on the WGS 84 ellipsoid model): the X-axis and Y-axis point toward the ellipsoid north (geodetic north) and the ellipsoid east (geodetic east), respectively. The Z-axis points downward along the ellipsoid normal. Coordinate vectors expressed in the local NED coordinate system are appended with a subscript n;
- *the aircraft-carried North-East-Down coordinate system* (denoted by  $O_{an} x_{an} y_{an} z_{an}$ ) is associated with the aircraft with origin (denoted by  $O_{an}$ ) located at the center of gravity (CG) of the aircraft. Its axes are given by the following (Fig. 5 and Fig. 4): the X-axis and Y-axis point toward the ellipsoid north (geodetic north) and the ellipsoid east (geodetic east), respectively. The Z-axis points downward along the ellipsoid normal. Coordinate vectors in the aircraft-carried NED system are denoted by a subscript an;
- *body coordinate system* (denoted by  $O_b x_b y_b z_b$ ) is directly defined on the body of the aircraft with the origin (denoted by  $O_b$ ) located at the CG (Fig. 4). The X-axis points forward, lying in the symmetric plane of the aircraft. The Y-axis points forward to the right side of the aircraft. The Z-axis points downward to comply with the right-hand rule. Coordinate vectors expressed in the body frame are described with a subscript b;
- *the head-fixed coordinate system* (denoted by  $O_h x_h y_h z_h$ ) is a frame with the origin (denoted by  $O_h$ ) fixed to the center of the head. The axes are defined through the coordinates of anatomical landmarks on the head: the Nasion (NAS), and the left and right preauricular points (LPA and RPA). The positive axes were directed nasally ( $x_h$ ), toward the right ear ( $y_h$ ), and toward the base of the skull ( $z_h$ ). Coordinate vectors expressed in the head frame are described with a subscript h.

The distance of the origin of the head-fixed frame ( $O_h x_h y_h z_h$ ) relative to the origin of the body frame ( $O_b x_b y_b z_b$ ) is determined by the vector  $\mathbf{I}_h$  (Fig. 4). This vector has two components  $\mathbf{I}_h = [l_{Hx_b}, 0, l_{Hz_b}]^T$  in the  $O_b x_b y_b z_b$  reference system.

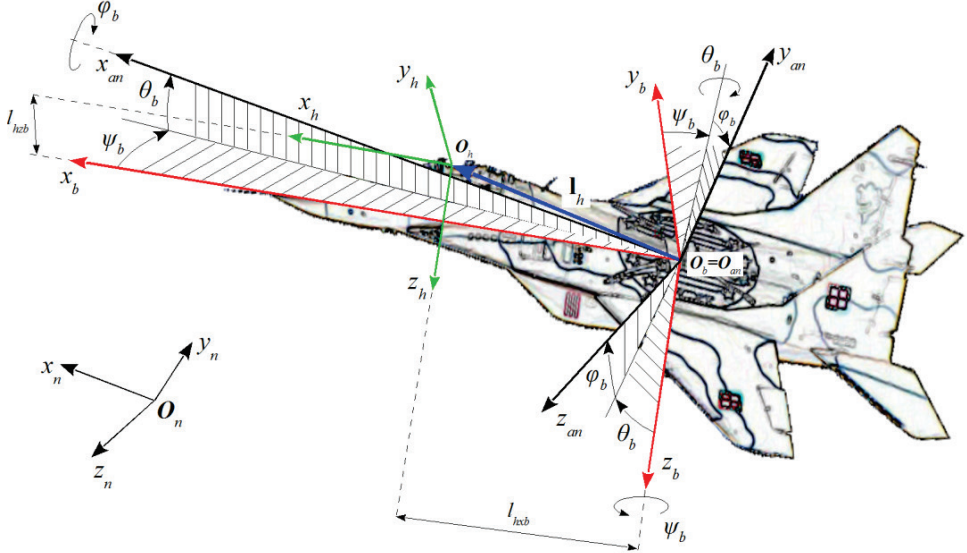


**Fig. 4.** The coordinate systems and the rotation angles

In addition to the linear acceleration of the aircraft recorded in the memory of the S2-3a FDR (Tab. 2), there may be additional centripetal and tangential components of linear acceleration acting on the pilot's head during an aircraft rotation ( $\Omega_b$ ). The resultant acceleration is therefore the sum of the three accelerations:

$$\mathbf{a}_h^{ac} = \mathbf{a}_b + \mathbf{a}_\epsilon + \mathbf{a}_\Omega \quad (2)$$

where

- $\mathbf{a}_b = [a_{x_b}, a_{y_b}, a_{z_b}]^T$  is the absolute acceleration of the aircraft's CG as recorded by the S2-3a FDR (Tab. 2).
- $\mathbf{a}_\epsilon = \boldsymbol{\epsilon}_b \times \mathbf{l}_h$  is the tangential acceleration, whose components are as follows:

$$\begin{aligned} a_{\epsilon x_b} &= \dot{q}_b \cdot l_{hz_b} - \dot{r}_b \cdot l_{hy_b} \\ a_{\epsilon y_b} &= \dot{r}_b \cdot l_{hx_b} - \dot{p}_b \cdot l_{hz_b} \\ a_{\epsilon z_b} &= \dot{p}_b \cdot l_{hy_b} - \dot{q}_b \cdot l_{hx_b} \end{aligned} \quad (3)$$

- $\mathbf{a}_\Omega = \boldsymbol{\Omega}_b \times (\boldsymbol{\Omega}_b \times \mathbf{l}_h)$  is a centripetal acceleration with components:

$$\begin{aligned} a_{\Omega x_b} &= p_b(p_b \cdot l_{hx_b} + q_b \cdot l_{hy_b} + r_b \cdot l_{hz_b}) - \Omega_b^2 \cdot l_{hx_b} \\ a_{\Omega x_b} &= q_b(p_b \cdot l_{hx_b} + q_b \cdot l_{hy_b} + r_b \cdot l_{hz_b}) - \Omega_b^2 \cdot l_{hy_b} \\ a_{\Omega x_b} &= r_b(p_b \cdot l_{hx_b} + q_b \cdot l_{hy_b} + r_b \cdot l_{hz_b}) - \Omega_b^2 \cdot l_{hz_b} \end{aligned} \quad (4)$$

in which the components of the pilot's head position vector are equal to  $\mathbf{l}_h = [1.35 \ 0 \ 4.25]^T$  (Fig. 4). The vector  $\mathbf{l}_h$  takes into account the translational displacement of the head resulting from the inclination of the seat backrest by an angle of 18 deg.

As a result, the acceleration  $\mathbf{a}_h^{ac}$  (2) acting on the pilot's head in the aircraft has the following components in the  $O_hx_hy_hz_h$  system:

$$\begin{aligned} a_{x_h}^{ac} &= a_{x_b} + \dot{q}_b l_{hz_b} - \dot{r}_b l_{hy_b} + p_b(p_b l_{hx_b} + q_b l_{hy_b} + r_b l_{hz_b}) - \Omega_b^2 l_{hx_b} \\ a_{y_h}^{ac} &= a_{y_b} + \dot{r}_b l_{hx_b} - \dot{p}_b l_{hz_b} + q_b(p_b l_{hx_b} + q_b l_{hy_b} + r_b l_{hz_b}) - \Omega_b^2 l_{hy_b} \\ a_{z_h}^{ac} &= a_{z_b} + \dot{p}_b l_{hy_b} - \dot{q}_b l_{hx_b} + r_b(p_b l_{hx_b} + q_b l_{hy_b} + r_b l_{hz_b}) - \Omega_b^2 l_{hz_b} \end{aligned} \quad (5)$$

Due to the lack of data on the angular position of the pilot's head during the actual flight, it was assumed that he/she did not make head movements, then:  $\phi_{h/n} = \phi_{b/n}$ ,  $\theta_{h/n} = \theta_{b/n}$ ,  $\psi_{h/n} = \psi_{b/n}$  and  $\Omega_h^{ac} = \Omega_b$  (Tab. 3).

## 2.5. The geodetic coordinates of the aircraft position

According to vector  $\mathbf{b}$  (1), to recreate the flight scenery (out of the window) in the HTC-07 simulator, the geodetic coordinates of the aircraft position are required (Table 2). This data is not recorded in the memory of the FDR (S2-3a) of the MiG-29 aircraft, but it can be determined by transforming the coordinates of the aircraft's position, described in the aircraft-carried NED coordinate system  $O_anx_any_anz_an$  (Fig. 5 and Fig. 4) to the geodetic coordinate system. To describe this transformation, the following rectangular and right-handed coordinate systems are defined (Fig. 5):

- *the geodetic coordinate system* – the frame that characterizes a coordinate point near the earth's surface in terms of longitude, latitude, and height (or altitude), which are respectively denoted by  $\lambda$ ,  $\phi$ , and  $h$ , see Fig. 5);
- *the earth-centered earth-fixed (ECEF) coordinate system* ( $O_ex_ey_ez_e$ ) with the origin (denoted by  $O_e$ ) located at the center of the earth (Fig. 5). The ECEF coordinate system rotates with the earth around its spin axis. The axes of the system are defined as follows: the X-axis coincides with the prime meridian (Greenwich meridian), the Z-axis is along the spin axis of the earth, pointing to the north pole, and the Y-axis is orthogonal to the Z- and X-axes with the right-hand rule (passes through the equator 90 degrees east of the prime meridian). Coordinate vectors in the ECEF frame is denoted by a subscript e.

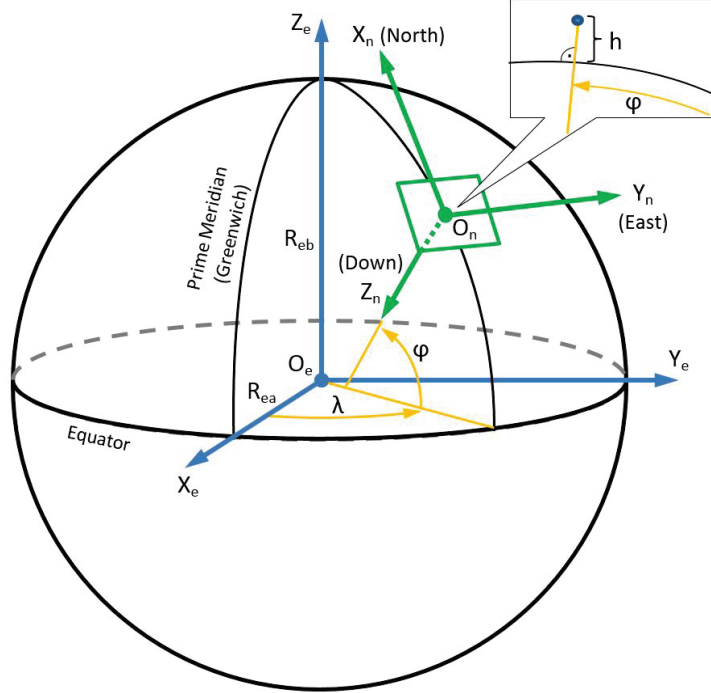


**Fig. 5.** Geodetic, ECEF  $O_e x_e y_e z_e$ , and local NED  $O_n x_n y_n z_n$  coordinate systems

The missing components  $(\varphi, \lambda)$  of vector  $\mathbf{b}$  (1) can be determined by knowing the initial geodetic position  $(\varphi_0, \lambda_0)$  and the change in this position over time. The derivative of the geodetic position can be expressed in terms of the velocity vector  $\mathbf{V}_{nv} = [u_{nv}, v_{nv}, w_{nv}]$  in the local NED  $O_n x_n y_n z_n$  coordinate system as follows [31], [32]:

$$\frac{d\lambda}{dt} = \frac{v_{nv}}{(N_e + h) \cos \varphi} \quad (6)$$

$$\frac{d\varphi}{dt} = \frac{u_{nv}}{M_e + h} \quad (7)$$

$$\frac{dh}{dt} = -w_{nv} \quad (8)$$

where

$\varphi$  – geodetic latitude (positive north);

$\lambda$  – geodetic longitude (measured from the Greenwich meridian);

$h$  – altitude normal to ellipsoid;

$N_e = \frac{R_{ea}}{\sqrt{1-e^2 \sin^2 \varphi}}$  – the prime vertical radius of curvature;

$M_e = \frac{R_{EA}(1-e^2)}{(1-e^2 \sin^2 \varphi)^{3/2}}$  – the meridian radius of curvature;

$R_{ea} = 6,378,137.0\text{ m}$  – the semi-major axis (ellipsoidal equatorial radius);

$R_{eb} = 6,356,752.0\text{ m}$  – the semi-minor axis;

$e = 0.08181919$  – the first eccentricity of ellipsoid;

The above mentioned parameters (and Fig. 5) are either defined or derived based on the WGS 84 (world geodetic system 84) ellipsoid model.

$u_{nv}, v_{nv}, w_{nv}$  – velocities in the aircraft-carried NED  $O_n x_n y_n z_n$  system, for which the derivatives are determined by [32]:

$$\frac{du_{nv}}{dt} = -\frac{v_{nv}^2 \sin \varphi}{(N_e + h) \cos \varphi} + \frac{u_{nv} w_{nv}}{M_e + h} + a_{xb/an} \quad (9)$$

$$\frac{dv_{nv}}{dt} = \frac{u_{nv} v_{nv} \sin \varphi}{(N_e + h) \cos \varphi} + \frac{u_{nv} w_{nv}}{N_e + h} + a_{yb/an} \quad (10)$$

$$\frac{dw_{nv}}{dt} = -\frac{v_{nv}^2}{N_e + h} + \frac{u_{nv}^2}{M_e + h} + g + a_{zb/an} \quad (11)$$

where  $g$  is the gravitational acceleration, and  $a_{b/an} = [a_{x_b/an} \ a_{y_b/an} \ a_{z_b/an}]$  is the projection of vector  $\mathbf{a}_b$  (the proper acceleration measured on the body  $O_b x_b y_b z_b$  frame and recorded in the FDR, Tab. 3) onto the aircraft-carried NED  $O_{an} x_{an} y_{an} z_{an}$  system. In the above equations (6-11), terms related to the earth's self-rotation were omitted.

The transformation of the acceleration vector between the aircraft-carried NED  $O_{an} x_{an} y_{an} z_{an}$  system and the body frame is as follows:

$$\begin{bmatrix} a_{x_b} \\ a_{y_b} \\ a_{z_b} \end{bmatrix} = \mathbf{L}_{b/an} \cdot \begin{bmatrix} a_{x_{an}} \\ a_{y_{an}} \\ a_{z_{an}} \end{bmatrix} \quad (12)$$

where  $\mathbf{L}_{b/an}$  is the rotation matrix from the aircraft-carried NED  $O_{an} x_{an} y_{an} z_{an}$  frame to the body  $O_b x_b y_b z_b$  frame and is given by:

$$\mathbf{L}_{b/an} = \begin{bmatrix} c\theta_b \cdot c\psi_b & c\theta_b \cdot s\psi_b & -s\theta_b \\ s\phi_b \cdot s\theta_b \cdot c\psi_b - c\phi_b \cdot s\psi_b & s\phi_b \cdot s\theta_b \cdot s\psi_b + c\phi_b \cdot c\psi_b & s\phi_b \cdot c\theta_b \\ c\phi_b \cdot s\theta_b \cdot c\psi_b + s\phi_b \cdot s\psi_b & c\phi_b \cdot s\theta_b \cdot s\psi_b - s\phi_b \cdot c\psi_b & c\phi_b \cdot c\theta_b \end{bmatrix} \quad (13)$$

where  $s$  and  $c$  denote  $\sin()$  and  $\cos()$ , respectively.

The inverse matrix  $\mathbf{L}_{b/an}^{-1} = \mathbf{L}_{an/b}$  provides a transformation of the acceleration vector from the body  $O_b x_b y_b z_b$  frame to the aircraft-carried NED  $O_{an} x_{an} y_{an} z_{an}$  coordinate frame (9-11).

## 2.6. Flight data processing

Due to the fact that the data recording in the S2-3a recorder of the MiG-29 aircraft took place at a frequency of 1 Hz (Tab. 3), which is lower than the frequency required for replication in the HTC-07 simulator (Tab. 2, frequency of 200 Hz), the data from the actual flight was linearly interpolated (function `interp1()` from the MATLAB package (MathWorks Inc., USA)). In addition, unit conversions were carried out, as listed in Table 2. A list of these conversions is shown in Table 4.

**Table 4**

### List of unit conversions of the actual flight data of the MiG-29 aircraft

Parameter	Name in the source file		
	MiG-29	Conversion type	HTC-07
Linear acceleration	$a_{x_c}^{htc}$	Nx	$g \rightarrow m/s^2$
	$a_{y_c}^{htc}$	<td>MSIout.Motion.f_y_b</td>	MSIout.Motion.f_y_b
	$a_{z_c}^{htc}$	Nz	MSIout.Motion.f_z_b
Altitude	Hbar	feet → meters	MSIout.OTW.h_eye
Roll angle	Gamma		MSIout.OTW.phi
Pitch angle	Theta	degree → radian	MSIout.OTW.theta
Yaw angle	Psi		MSIout.OTW.psi

## 2.7. Flight parameter vector recreated in the simulator

The final step of the actual flight replication was preceded by checking the procedure for recreating the vector **b** (1) in the HTC-07 simulator offline (with the motion system deactivated). Successful completion of this procedure, confirmed by correctly displaying the flight scenery and flight parameters indicators, was a prerequisite for a full (with active the motion system) replication of the actual flight. In the case of failure, the recheck of the format data and range of values of the components of vector **b** (1) were performed.

As a result of replicating the real flight (vector **b**) in the HTC-07 simulator, the vector **k**, which describes the kinematics of the simulator cabin, was created. This vector has the following components in the pilot's head-fixed  $O_h x_h y_h z_h$  coordinate frame:

$$\mathbf{k} = [\phi_{h/n}^{htc}, \theta_{h/n}^{htc}, \psi_{h/n}^{htc}, a_{x_h}^{htc}, a_{y_h}^{htc}, a_{z_h}^{htc}, p_h^{htc}, q_h^{htc}, r_h^{htc}]^T \quad (14)$$

A detailed description of these components is given in Table 5.

**Table 5**

**Kinematics parameters of the HTC-07 simulator (see Fig. 6)**

Parametr	Unit	Reference frame	Component of vector $\mathbf{k}$	Name in the source file
Ring roll angle $\phi_R^{htc}$			$\phi_{h/n}^{htc}$	general.SysInput.DPLCout.Alpha.alpha
Cabin pitch angle $\theta_C^{htc}$	rad	$O_n x_n y_n z_n$	$\theta_{h/n}^{htc}$	general.SysInput.DPLCout.Beta.beta
Arm yaw angle $\psi_A^{htc}$			$\psi_{h/n}^{htc}$	general.SysInput.DPLCout.Phi.phi
Linear acceleration	$\frac{a_{x_c}^{htc}}{g}$	$Cx_C y_C z_C$ *	$\mathbf{a}_h^{htc}$	general.SysInput.DPLCout.Indications.Gx general.SysInput.DPLCout.Indications.Gy general.SysInput.DPLCout.Indications.Gz
Angular velocity	$\frac{\text{ring } p_R^{htc}}{\text{cabin } q_C^{htc}}$ rad/s	$Rx_R y_R z_R$ * $Cx_C y_C z_C$ * $\Omega_C^{htc}$ **		general.SysInput.DPLCout.Alpha.dalpha general.SysInput.DPLCout.Beta.dbeta general.SysInput.DPLCout.Phi.dphi
	$a_{z_c}^{htc}$	$Ax_A y_A z_A$ *		

\* – coordinate system defined in the following subsection and in Fig. 6

\*\* – vector calculated using the relationships presented in the following subsection

Given the influence of aircraft angular velocities on the pilot's ability to maintain spatial orientation, and linear acceleration, high fidelity of the angular velocities generated in the HTC-07 simulator is also expected. The angular velocity vector acting on the pilot's head in the simulator  $\Omega_C^{htc} = [p_C^{htc}, q_C^{htc}, r_C^{htc}]^T$  (14) is the sum of the angular velocity of the arm  $r_A^{htc}$ , the ring  $p_R^{htc}$ , and the cabin  $q_C^{htc}$  (Tab. 5), transformed to the simulator cabin-fixed coordinate system (the system defined below). To derive these angular velocity vector components, the following right-handed, orthogonal coordinate systems are applied (Fig. 6):

- the local North-East-Down (NED) coordinate system ( $O_n x_n y_n z_n$ ) – previously defined in Fig. 5 and Fig. 4, with the origin fixed to a point on the earth's surface, in the rotation axis of the simulator arm,
- the arm-fixed coordinate system (denoted by  $Ax_A y_A z_A$ ) with the origin (denoted by  $A$ ) of the intersection of the rotation axis of the ring and the simulator cabin. The values expressed in this system are indicated by the subscript A,
- the ring-fixed coordinate system (denoted by  $Rx_R y_R z_R$ ) with the origin (denoted by  $R$ ) that aligns with the origin of the  $Ax_A y_A z_A$  system. The  $Rx_R$  axis aligns with the  $Ax_A$  axis of the arm-fixed frame, while the  $Ry_R$  axis is the rotation axis of the cabin. The values expressed in the ring-fixed frame are distinguished by the subscript R,

- the cabin-fixed coordinate system (denoted by  $Cx_Cy_Cz_C$ ) with the origin (denoted by  $C$ ) that aligns with the origin of the  $Ax_Ay_Az_A$  system. The  $Cy_C$  axis is the rotation axis of the cabin and aligns with the  $Ry_R$  axis of the system associated with the ring. The values expressed in this system are marked with the subscript  $C$ ,
- the head-fixed coordinate system ( $O_hx_hy_hz_h$ ) previously defined in Fig. 4, with the origin (denoted by  $O_h$ ) is fixed to the center of the head and aligned with the origin of the cabin-fixed coordinate system. The axes of the  $O_hx_hy_hz_h$  axes align with the axes of the  $Cx_Cy_Cz_C$  system.

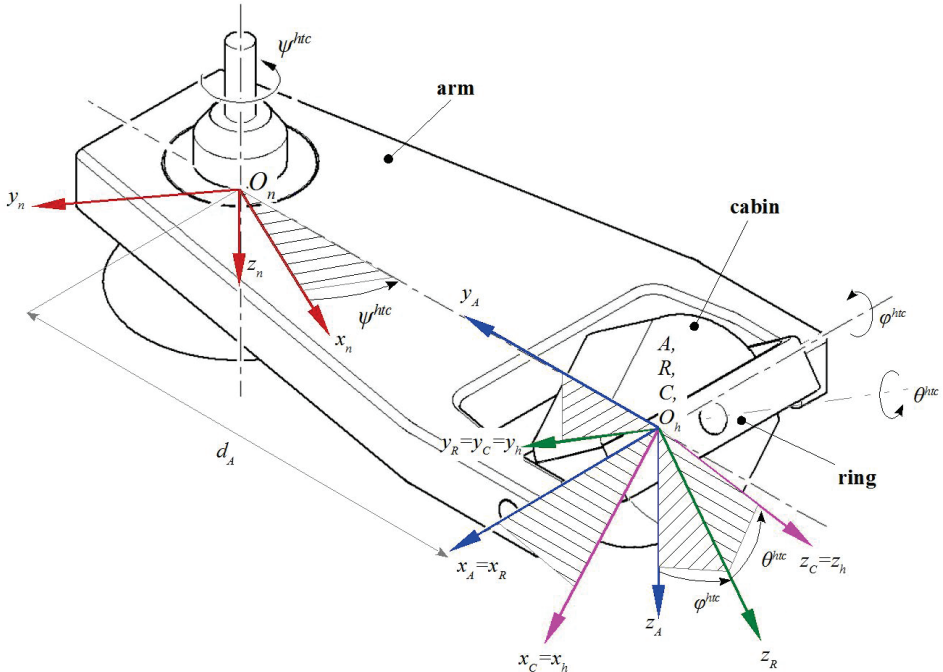


**Fig. 6.** Coordinate systems of the HTC-07 simulator and the transition angles between them [26]

The pilot's seat in the simulator cabin at a backrest tilt angle of  $\theta_h = 0$  degrees allows the origin of the head-fixed coordinate system ( $O_hx_hy_hz_h$ ) to be aligned with the origin of the cabin-fixed system ( $Cx_Cy_Cz_C$ ). To replicate the flight of the MiG-29 aircraft in the HTC-07 simulator, it is required to set the backrest at a backward tilt angle of  $\theta_h = 18$  degrees. With this seat configuration, there is an offset between the above-mentioned coordinate system origins. However, the design of the seat provides allows to change its forward-backward and upward-backward position, and eliminate this offset, which was done in the presented calculations.

Assuming, as in a real flight, that the pilot does not move his head (either linear or angular) relative to the cabin during flight in the simulator, then  $\Omega_h = \Omega_C$ . Thus, the

components of the angular velocity vector acting on the pilot's head in the cockpit of the HTC-07 simulator are described by the relations [26] and [33]:

$$\begin{bmatrix} p_h^{htc} \\ q_h^{htc} \\ r_h^{htc} \end{bmatrix} = \begin{bmatrix} \dot{\phi}^{htc} \cdot \cos \theta^{htc} - \dot{\psi}^{htc} \cdot \cos \phi^{htc} \cdot \sin \theta^{htc} \\ \dot{\theta}^{htc} + \dot{\psi}^{htc} \cdot \sin \phi^{htc} \\ \dot{\phi}^{htc} \cdot \sin \theta^{htc} + \dot{\psi}^{htc} \cdot \cos \phi^{htc} \cdot \cos \theta^{htc} \end{bmatrix} \quad (15)$$

where

$\phi^{htc}$ ,  $\theta^{htc}$  are roll and pitch angle, respectively (Fig. 6);

$\dot{\psi}^{htc}$ ,  $\dot{\phi}^{htc}$  and  $\dot{\theta}^{htc}$  are the angular velocities of the arm, the ring and the cab of the simulator, respectively.

## 2.8. Quality indicators for replicating a real flight in the simulator

The root mean square percentage error (RMSPE) and the Pearson's type correlation coefficient  $r_{bk}$  were used to compare the components of the **k** (14) and **b** (1) vectors and calculate replication accuracy. The RMSPE is a measure of the average deviation of an observation (the real flight) to its replicated value (in the simulator). It was used to aggregate the deviations (error values between the component of vector **b** and the corresponding component of vector **k**) into a single measure of compliance power. The smaller the deviations, the smaller the RMSPE and, thus, the more accurate the simulator's representation of the parameter being compared. The RMSPE was calculated using the following equation:

$$RMSE_i = \sqrt{\frac{1}{N} \cdot \sum_{n=1}^N \left( \frac{b_i(n) - k_i(n)}{b_i(n)} \right)^2} \cdot 100\% \quad (16)$$

where

$i$  – component of the vector

N – number of data samples of the vector component

$k_i(n)$  –  $i$ -th component of the simulator cabin kinematics vector

$b_i(n)$  –  $i$ -th component of the actual flight vector

The correlation coefficient  $r_{bk}$  shows the shape dependency of two signals (the analyzed components of vectors **b** and **k**) regardless of their magnitude. This coefficient was calculated as follows:

$$r_{bki} = \frac{\sum_{n=1}^N [b_i(n) - \bar{b}_i] \cdot [k_i(n) - \bar{k}_i]}{\sqrt{\sum_{n=1}^N [b_i(n) - \bar{b}_i]^2} \cdot \sqrt{\sum_{n=1}^N [k_i(n) - \bar{k}_i]^2}} \quad (17)$$

where

$i$  – component of the vector

$N$  – number of data samples of the vector component  
 $b_i, k_i$  –  $i$ -th component of the vector of the actual flight and the simulator cabin kinematics, respectively  
 $\bar{b}_i, \bar{k}_i$  – mean value of the  $i$ -th component of the vector.

The correlation coefficient reaches values ranging from -1 to 1. An increased correlation coefficient indicates the HTC-generated signal to follow the real signal shape more accurately. When  $r_{bk} = 1$  or -1, it means that two signals are completely following each other.

### 3. Results and discussion

All calculations, including the creation of the  $\mathbf{b}$  and  $\mathbf{k}$  vector components and the data file replicated in the HTC-07 simulator, were performed using MATLAB software (MathWorks Inc., US). The pretests confirmed the correct structure and format of vector  $\mathbf{b}$  and that its components did not exceed the range of acceptable values for the HTC-07 simulator.

The results of comparing components of the vector  $\mathbf{k}$  with vector  $\mathbf{b}$  (RMSPE and correlation coefficient  $r_{bk}$ , calculated using equations (16) and (17), respectively) are shown in Table 6. These results are discussed later in this chapter in the description of the analyzed parameters.

**Table 6**  
**Results of quantitative evaluation of the replication of selected parameters of the real flight in the HTC-07 simulator**

Parameter	Components of the vector	RMSPE	Correlation coefficient r
Linear acceleration (m/s <sup>2</sup> )	$a_{x_h}$	14 205	0.31
	$a_{y_h}$	10 889	-0.02
	$a_{z_h}$	2 068	0.98
Angular velocity (deg/s)	$p_h$	12 640	-0.02
	$q_h$	383 386	0.83
	$r_h$	267 956	-0.31

RMSPE – root mean square percentage error; r – Pearson's correlation coefficient

As a result of replicating the real flight of the MiG-29 aircraft in the HTC-07 simulator, the linear acceleration and angular velocity (calculated from the recorded angular velocities of the arm, ring and cabin as well as their orientation Eq. (15)) acting on the pilot's head

were recorded, and together with corresponding the real flight parameters are shown in Figs. 7 and 8. The components of the vector  $\mathbf{b}$  (1) of the real flight parameters are shown in blue. In contrast, the components of the vector  $\mathbf{k}$  (14), which describes the kinematics of the simulator cabin during the replication of this flight, are shown in red.

### 3.1. Recreation of the linear acceleration

The components of the linear acceleration vector acting on the pilot's head in the actual flight and during the replication of this flight in the HTC-07 simulator are shown in Fig. 7 in blue and red lines, respectively. These accelerations do not include the gravitational acceleration component.

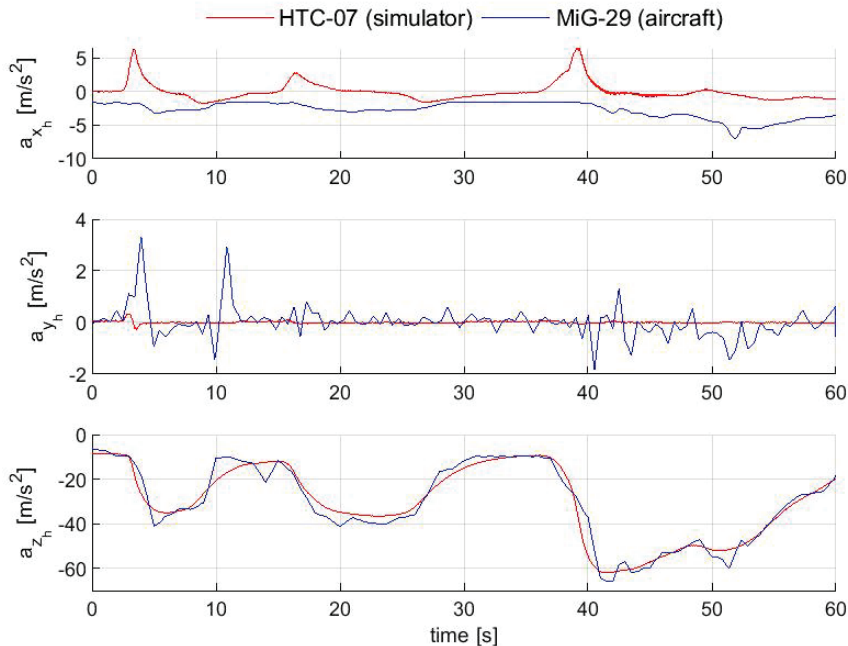


**Fig. 7.** The linear acceleration vector components acting on the pilot's head in the real flight and during the replication of this flight in the HTC-07 simulator (vector in the head-fixed coordinate system)

A clear match of the acceleration signals can be seen in the  $a_{z_h}$  component which, as in an aircraft flight, is the linear acceleration component that dominates in the simulator [34], [35]. This is confirmed by quantitative accuracy indicators (Table 6). The component  $a_{z_h}$  achieved the lowest RMSPE and the highest value of correlation coefficient  $r_{bkz_h} = 0.98$  among the analyzed acceleration components.

The largest differences in the replication of linear acceleration occurred for the  $a_{x_h}$  component (Table 6). These differences (around the 5th, 15th and 40th second of the analyzed flight profile, Fig. 7) relate to the method used to compensate for unwanted tangential acceleration in the simulator motion system control algorithm. The tangential acceleration occurs when the rotational velocity of the simulator arm changes ( $a_x = \epsilon_A \cdot d_A$ ); therefore when the generated G-force ( $a_{z_h}$ ) changes (Fig. 7), the pitch angle  $\theta^{htc}$  of the cabin is applied to reduce this tangential acceleration. As a result, artefacts also occurred in the vertical component  $a_{z_h}$  of the generated linear acceleration (Fig. 7).

In the case of the  $a_{y_h}$  components the largest differences occurred around the 5th, 10th and 40th second of the analyzed flight profile (Fig. 7). The reason for these differences can be attributed to the turn maneuver which, as can be seen in Fig. 8, was performed with a roll rate  $p_{an}$  that reached 60 deg/s. According to the signal shown in Fig. 3, this turn was maintained until the 5th second of the flight with a roll angle  $\phi_{an}$  close to 90 deg. At about 10th second, there was a change in the roll angle, of almost 180 degrees, to a turn to the other side. During roll angle change, the linear acceleration replicated in the simulator (red line) compared to the acceleration recorded during the real flight (blue line) shows a clear difference for the components  $a_{x_h}$  and  $a_{y_h}$ .

Although all components of linear acceleration generated in the simulator do not exactly match the signals recorded in the real flight (Fig. 7), the maximum values of these accelerations and their change rate are particularly relevant for assessing a pilot's in-flight behavior. Lambert [36], [37] found that visual disturbances in flight occur at higher acceleration values than during training in centrifuges. This difference is about 0.7 G and, according to the author, depends on the difference in the level of emotional tension in the two situations and on the flight conditions (active mode, when a pilot controls a flight vs passive mode when a pilot has no influence on the flight and the generated acceleration).

### 3.2. Recreation of the angular velocity

The components of the angular velocity vector acting on the pilot's head in a real flight of the MiG-29 aircraft and during the replication of this flight in the HTC-07 simulator are shown in Fig. 8 in blue and red lines, respectively.

Comparing the angular velocity components replicated in the simulator with the data recorded during the real flight (Fig. 8), it is evident that the roll angular velocity  $p_h$  exhibits no significant difference. This observation was confirmed by the RMSPE value (Table 6). In the case of the other two components (pitch  $q_h$  and yaw  $r_h$  rates), a large difference can be seen (Fig. 8, blue vs. red line). These components of angular velocity constantly act on the pilot's head. Their occurrence is related to the rotation of the simulator arm and the cabin roll angle  $\phi^{htc}$ . The latter has the task of bringing the centripetal and gravitational

accelerations to the resultant acceleration. For example, for the +2 Gz acceleration generated in the simulator, the cabin roll angle is set to  $\phi^{htc} = 58$  deg.

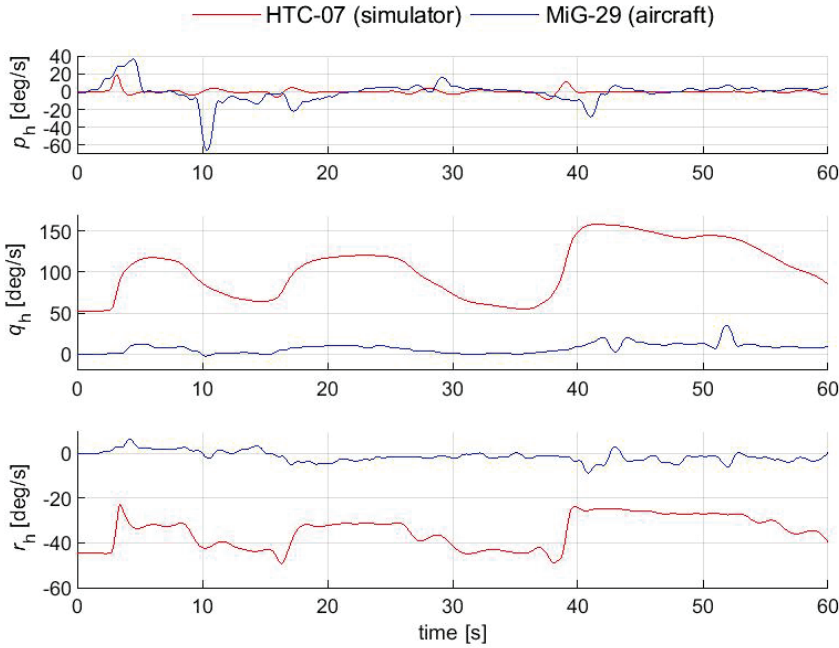


**Fig. 8.** The angular velocity vector components recorded in a real flight and during the reproduction of this flight in the HTC-07 simulator (vector in the head-fixed coordinate system)

The observed differences in the angular velocity components (Fig. 8, Table 6) replicated in the HTC-07 simulator are due to the fact that these parameters are not required to recreate the flight (Table 3). The angular velocity generated by the simulator is a side-effect of how the simulator's motion system generates linear acceleration. However, taking into account the physiology of the human vestibular system, with the receptor responsible for detecting angular acceleration, the differences observed between the angular velocities in the real flight and those replicated in the simulator (Fig. 8) may not be perceived by the pilot. For a constant angular velocity, the vestibular system gives a misleading sensation of diminishing rotational motion [38]. Therefore, since the angular velocity of the simulator arm, the cabin's roll angle and the pilot's head are all constant, the pilot should not perceive the sensation of rotation. The change in angular velocity of the arm only appears when the linear acceleration generated by the simulator is suddenly increased or decreased (see Fig. 8 in the 5th, 10th, 17th and 39th second). In such cases, the pilot may perceive a rotational motion that would not occur during the real flight.

Although none of the linear acceleration components were replicated with a high level of fidelity, the acceleration  $a_{zh}$  is the closest to the results from the real flight (Fig. 7, Table 6). For the angular velocities, the HTC-07 simulator showed low-fidelity replication (Fig. 8, Table 6). Although the simulator can replicate the linear acceleration, it generates additional motion stimuli (e.g. pitch and yaw rates, Fig. 8), giving the pilot sensations that he or she would not have experienced in the real flight. If the simulator could replicate the angular velocity more precisely, it could be utilized to investigate aviation accidents where the pilot's perceptual errors may have contributed to spatial disorientation during flight [39].

However, the HTC-07 simulator's low level of fidelity in replicating the other components of linear acceleration and angular velocity does not disqualify its use in aircraft accident investigations. This is because the pilot's visual disturbances and G-LOC are primarily influenced by the vertical component of the linear acceleration  $a_{zh}$ .

### **3.3. The simulator limitations**

This study highlights several concerns that indicate a limited capacity for a centrifuge-based flight simulator to recreate real-world flight scenarios. Specifically, a core contrast exists between a real flight with six degrees of freedom and the three degrees of freedom environment available in a centrifuge simulator. While the main purpose of this simulator is to generate linear accelerations that mimic those experienced during flight, its accuracy in replication is not optimized. This limitation primarily relates to the technique of simulating flight conditions with accelerations below +1.4 Gz.

Another imperfection of centrifuge-based simulators are artefacts in the form of motion stimuli that do not occur in simulated real flight. The assumption made in this study that the pilot does not make any head movements during the simulated flight in the centrifuge should exclude at least one group of these stimuli.

This is a simplifying assumption since head movements are common during flight, particularly when engaging in dogfights in the MiG-29 fast-jet. When simulating flight in a centrifuge, the movement of the head during the rotation of the simulator's arm stimulates all three semicircular canals of the vestibular system simultaneously, leading to unpleasant motion sensations in pilots. These sensations can trigger motion sickness, commonly referred to as simulator sickness in simulator environments.

## **4. Conclusions and summary**

This study aimed to replicate the real flight of the MiG-29 aircraft using a centrifuge-based dynamic flight simulator and to determine the simulator's accuracy in recreating in-flight aircraft performance.

The study demonstrated that replicating the actual flight in the HTC simulator is not challenging. The presented method of flight replication could prove to be a valuable tool to support future accident investigations. The HTC-07 simulator is able to accurately replicate the aircraft in-flight performance with respect to the vertical component of the linear acceleration ( $a_{zh}$ ). Unfortunately, the anticipated high fidelity was not achieved in replicating any of the angular velocity components. Nevertheless, the inaccuracy in replicating the other components of this acceleration and the angular velocity does not exclude the use of the simulator in the investigation of events related to human factors. It is mainly due to the pilot's visual disturbance and loss of consciousness, which are related to the vertical component of the linear acceleration ( $a_{zh}$ ).

A data-driven approach to investigating aviation accidents, as demonstrated in this study, can provide valuable insight into the cause of an accident and hence may contribute to reducing the number of accidents. The replication of the MiG-29 aircraft flight in the HTC-07 simulator was based on data from the S2-3a flight data recorder. This particular recorder is not only used in MiG-29 aircraft but also in various other types of aircraft, such as TS-11 ISKRA, PZL-130 TC-II ORLIK, M-28 BRYZA, Su-22 and rotary-wing Mi-8, Mi-14, Mi-17, Mi-24, W-3 SOKOL, and SW-4 [40]. It means that the method used for processing data from this recorder can also be applied to analyze the flight performance of these aircraft.

When investigating accidents using a dynamic centrifuge-based flight simulator, it is essential to consider potential challenges in analyzing the effects of acceleration on a pilot. These challenges may be due to limited information about the anti-G straining maneuver. Delayed maneuver initiation, insufficient lower body muscle tension, or improper breathing techniques can decrease acceleration tolerance and increase the likelihood of experiencing G-LOC.

Based on data and lessons learned from past flight incidents and accidents, the HTC-07 simulator capability can provide a training environment for pilots. To enhance training and reduce aircraft accident rates, the requirements for such a simulation must be based on a clear specification of training needs.

Finally, the presented method for replicating the real flight in the HTC-07 simulator can be applied to centrifuge-based flight simulators used by other countries, such as the Indian Air Force, the Republic of Singapore Air Force, the German Air Force, and the UK Royal Air Force [41]. It should be noted that while dynamic flight simulators are recognized as valuable tools in aviation accident investigation, the limitations of these devices and their seemingly high level of fidelity in replicating the flight environment may lead an inexperienced investigator to draw erroneous conclusions.

## 5. References

1. B. Elias, "Flight Simulation as an Investigative Tool for Understanding Human Factors in Aviation Accidents," *Int. Symp. Aviat. Psychol.*, pp. 219–224, 2005.
2. M. C. Newman, B. D. Lawson, B. J. McGrath, and A. H. Rupert, "Perceptual modeling as a tool to prevent aircraft upset associated with spatial disorientation," in *Proceedings of the AIAA Guidance, Navigation, and Control Conference*, 2014, pp. 1–12. DOI: 10.2514/6.2014-0443.
3. R. Tydeman, "The Use of Full Flight Simulators for Accident Investigation," in *Proceedings of the 35th Annual International Seminar*, 2004, pp. 1–9.
4. D. Tran and E. Hernandez, "Use of the vertical motion simulator in support of the American airlines flight 587 accident investigation," in *AIAA Modeling and Simulation Technologies Conference and Exhibit*, 2004, pp. 1–7. DOI: 10.2514/6.2004-5032.
5. A. Vidovic, A. Franjic, I. Štimac, and M. O. Ban, "The Importance of Flight Recorders in the Aircraft Accident Investigation," *Transp. Res. Procedia*, vol. 64, no. C, pp. 183–190, 2022, DOI: 10.1016/j.trpro.2022.09.022.
6. L. M. Saele and W. B. Webb, "Use of accident data, instructors' comments and students' responses in transition flight training.,," *J. Aviat. Med.*, vol. 29, no. 11, pp. 805–809, 1958.
7. M. Rey, D. Aloise, F. Soumis, and R. Pieugueu, "A data-driven model for safety risk identification from flight data analysis," *Transp. Eng.*, vol. 5, p. 100087, Sep. 2021, DOI: 10.1016/J.TRENG.2021.100087.
8. D. A. Wiegmann and S. A. Shappell, *A human error approach to aviation accident analysis: the human factors analysis and classification system*. Ashgate, 2003.
9. D. A. Wiegmann and S. A. Shappell, "Human error analysis of commercial aviation accidents: Application of the human factors analysis and classification system (HFACS)," *Aviat. Sp. Environ. Med.*, vol. 72, no. 11, pp. 1006–1016, 2001.
10. M. Wojtkowiak, *Badanie tolerancji ustroju na działanie przyspieszeń na podstawie oceny prędkości przepływu krwi w tętnicy skroniowej i zaburzeń wzrokowych*. Warszawa: Wojskowy Instytut Medycyny Lotniczej, 1982.
11. E. H. Wood, "G-Induced Loss of Consciousness and Its Prevention. USAFSAM-TR-87-41," Brooks Air Force Base, TX, 1988.
12. O. Truszczyński, M. Wojtkowiak, R. Lewkowicz, M. P. Biernacki, and K. Kowalcuk, "Reaction time in pilots at sustained acceleration of +4.5 Gz," *Aviat. Space. Environ. Med.*, vol. 84, no. 8, pp. 845–849, 2013, DOI: 10.3357/asem.3490.2013.

13. O. Truszczyński, R. Lewkowicz, M. Wojtkowiak, and M. P. Biernacki, “Reaction time in pilots during intervals of high sustained G,” *Aviat. Sp. Environ. Med.*, vol. 85, no. 11, pp. 1114–1120, 2014, DOI: 10.3357/ASEM.4009.2014.
14. U. I. Balldin, G. Derefeldt, L. Eriksson, P. M. Werchan, P. Andersson, and J. T. Yates, “Color vision with rapid-onset acceleration,” *Aviat. Space. Environ. Med.*, vol. 74, no. 1, pp. 29–36, Jan. 2003.
15. D. Randjelović and M. Pavlović, “The effect of acceleration on color vision,” *Vojnosanit. Pregl.*, vol. 75, no. 6, pp. 623–627, Jun. 2018, DOI: 10.2298/VSP160622288R.
16. W. J. White, “Variations In Absolute Visual Thresholds During Acceleration Stress. (ASD-TR-60-34, DTIC No. AD0243612),” Wright-Patterson Air Force Base, OH, 1960.
17. A. L. Comrey, A. A. Canfield, R. C. Wilson, and W. S. Zimmerman, “The effect of increased positive radial acceleration upon perceptual speed ability.,” *J. Aviat. Med.*, vol. 22, no. 1, pp. 60–4, Feb. 1951.
18. O. Truszczyński, M. Wojtkowiak, M. P. Biernacki, K. Kowalcuk, and R. Lewkowicz, “Effect of high acceleration exposure on visual perception in Polish pilots measured with Critical Fusion Frequency Test (CFFT),” *Polish J. Aviat. Med. Psychol.*, vol. 1, no. 1, pp. 19–27, 2012.
19. E. Ercan and S. H. Gunduz, “The Effects of Acceleration Forces on Cognitive Functions,” *Microgravity Sci. Technol.*, vol. 32, no. 4, pp. 681–686, 2020, DOI: 10.1007/s12217-020-09793-0.
20. D. A. Tipton, A. R. Marko, and D. A. Ratino, “The effects of acceleration forces on night vision,” *Aviat. Sp. Environ. Med.*, vol. 55, no. 3, pp. 180–190, 1984.
21. I. Y. Akparibo, J. Anderson, and E. Chumbley, “Aerospace Gravitational Effects,” in *StatPearls [Internet Updated 2023 Aug 8]*, Treasure Island (FL): StatPearls Publishing LLC., 2023.
22. R. M. Chambers and L. Hitchcock, “Effects of acceleration on pilot performance. Tech. Rep. No. NADC-MA-6219,” Johnsville, PA, Mar. 1963. DOI: 10.21236/ad0408686.
23. C. L. Heaps, M. D. Fischer, and R. C. Hill, “Female acceleration tolerance: effects of menstrual state and physical condition,” *Aviat. Space. Environ. Med.*, vol. 68, no. 6, pp. 525–530, Jun. 1997.
24. R. Kölegård, I. B. Mekjavić, and O. Eiken, “Effects of physical fitness on relaxed G-tolerance and the exercise pressor response,” *Eur. J. Appl. Physiol.*, vol. 113, no. 11, pp. 2749–2759, 2013, DOI: 10.1007/s00421-013-2710-z.
25. R. M. Masica, “A study to evaluate the suitability of a centrifuge as a dynamic flight simulator for F/A-18 strike fighter mission training. MSc. thesis,” University of Tennessee, 2009.

26. R. Lewkowicz, “Dochodzenie w sprawie wypadku lotniczego z zastosowaniem dynamicznego symulatora lotu,” *Mechanika w Lotnictwie ML-XIX*, K. Sibilski and P. Lichota, Eds. Warszawa: Instytut Techniczny Wojsk Lotniczych, 2020, pp. 131–151. DOI: 10.15632/ML2020/131-151.
27. O. Truszczyński and K. Kowalcuk, “The polish centrifuge as a dynamic flight simulator. New application and ideas,” *Polish J. Aviat. Med. Psychol.*, vol. 18, no. 3, pp. 71–80, 2012.
28. AMST-Systemtechnik GmbH, “User manual Human Training Centrifuge HTC-07,” Amst-Systemtechnik GmbH, Austria, 2011.
29. A. Szelmanowski and Z. Jakielaszek, “Błędy skrośne w pomiarach parametrów ruchu statku powietrznego i możliwości ich korekcji,” *Pomiary, Autom. Kontrola*, vol. 53, no. 9, pp. 564–567, 2007.
30. A. Szelmanowski, “Metoda korekcji błędów skrośnych dla pomiarów parametrów ruchu w zintegrowanych systemach awionicznych,” *Res. Work. Air Force Inst. Technol.*, vol. 25, no. 1, pp. 209–223, 2009, DOI: 10.2478/v10041-009-0018-6.
31. A. Noureldin, T. B. Karamat, and J. Georgy, “Basic Navigation Mathematics, Reference Frame and the Earth’s Geometry,” in *Fundamentals of Inertial Navigation, Satellite-Based Positioning and their Integration*, Springer-Verlag Berlin Heidelberg, 2013, pp. 21–63. DOI: 10.1007/978-3-642-30466-8.
32. G. Cai, B. M. Chen, and T. H. Lee, “Coordinate systems and transformations,” in *Advances in Industrial Control*, no. 9780857296344, London, UK: Springer International Publishing, 2011, pp. 23–34. DOI: 10.1007/978-0-85729-635-1\_2.
33. R. Lewkowicz and G. Kowaleczko, “Kinematic issues of a spatial disorientation simulator,” *Mech. Mach. Theory*, vol. 138, pp. 169–181, 2019, DOI: 10.1016/j.mechmachtheory.2019.04.003.
34. E. Seedhouse, *Pulling G : human responses to high and low gravity*. Springer, 2013.
35. D. G. Newman and W. Tutton, *High G flight: physiological effects and countermeasures*, 1st ed., vol. 61, no. 3. Monash University, Australia: Ashgate Publishing Ltd, 2015. DOI: 10.1080/00140139.2017.1363547.
36. E. H. Lambert, “Comparison of the physiologic effect of positive acceleration on a human centrifuge and in an airplane,” *J. Aviat. Med.*, vol. 20, no. 5, pp. 308–335, Oct. 1949.
37. E. H. Lambert, “Effects of positive acceleration on pilots in flight with a comparison,” *J. Aviat. Med.*, vol. 21, no. 3, pp. 195–220, 1950.
38. R. Lewkowicz and G. Kowaleczko, Ocena jakości odwzorowania przyspieszeń w wirówce przeciążeniowej” *Mechanika w lotnictwie ML-XVIII*, K. Sibilski, Ed. Kazimierz Dolny: Polskie Towarzystwo Mechaniki Teoretycznej i Stosowanej, 2018, pp. 67–78.

39. R. Lewkowicz and M. P. Biernacki, “A survey of spatial disorientation incidence in Polish military pilots,” *Int. J. Occup. Med. Environ. Health*, vol. 33, no. 6, pp. 791-810, 2020, DOI: 10.13075/ijomeh.1896.01621.
40. Z. Jakielaszek and M. Nowakowski, “Studying the strength of an S2-3a flight data recording system flight recorder,” *Mechanik*, no. 4, pp. 6–12, 2020, DOI: 10.17814/mechanik.2020.4.9.
41. “High G Centrifuge Training,” *Indian J. Aerosp. Med.*, vol. 50, no. 1, pp. 1–7, 2006.

